

NOVEL CONSISTENCY CHECK FOR FAST RECURSIVE RECONSTRUCTION OF NON-REGULARLY SAMPLED VIDEO DATA

Simon Grosche, Jürgen Seiler, and André Kaup

Multimedia Communications and Signal Processing
Friedrich-Alexander-Universität Erlangen-Nürnberg, Cauerstr. 7, 91058 Erlangen, Germany
{simon.grosche, juergen.seiler, andre.kaup}@fau.de

ABSTRACT

Quarter sampling is a novel sensor design that allows for an acquisition of higher resolution images without increasing the number of pixels. When being used for video data, one out of four pixels is measured in each frame. Effectively, this leads to a non-regular spatio-temporal sub-sampling. Compared to purely spatial or temporal sub-sampling, this allows for an increased reconstruction quality, as aliasing artifacts can be reduced. For the fast reconstruction of such sensor data with a fixed mask, recursive variant of frequency selective reconstruction (FSR) was proposed. Here, pixels measured in previous frames are projected into the current frame to support its reconstruction. In doing so, the motion between the frames is computed using template matching. Since some of the motion vectors may be erroneous, it is important to perform a proper consistency checking. In this paper, we propose faster consistency checking methods as well as a novel recursive FSR that uses the projected pixels different than in literature and can handle dynamic masks. Altogether, we are able to significantly increase the reconstruction quality by +1.01 dB compared to the state-of-the-art recursive reconstruction method using a fixed mask. Compared to a single frame reconstruction, an average gain of about +1.52 dB is achieved for dynamic masks. At the same time, the computational complexity of the consistency checks is reduced by a factor of 13 compared to the literature algorithm.

Index Terms— Non-Regular Sampling, Image Reconstruction

1. INTRODUCTION

Using quarter sampling [1], the spatial resolution of an imaging sensor can be increased. This is achieved by physically covering three quarters of each pixel of a regular low-resolution sensor. Effectively, this leads to a non-regular sampling of the image with respect to a higher resolution grid with twice the resolution in both spatial dimensions as can be seen in Figure 1 (left). Due to the non-regularity, visually disturbing aliasing artifacts that conventionally occur for regular sampling can be reduced [2, 3, 4]. For the reconstruction, frequency selective reconstruction (FSR) has shown to be a successful reconstruction scheme for various inpainting and extrapolation tasks [5, 6] and gave best results for non-regular sampling and quarter sampling in [1, 7, 8]. Quarter sampling, as well as any non-regular sub-sampling, can be seen as a special case of compressed sensing [9, 10] as has been shown in [7, 11]. In the compressed sensing framework, the FSR can be interpreted as a special case of more general reconstruction algorithms from the class of matching pursuit algorithms [11, 12, 13].

Besides still images, the acquisition of video data is of great importance. In combination with quarter sampling, video acquisi-

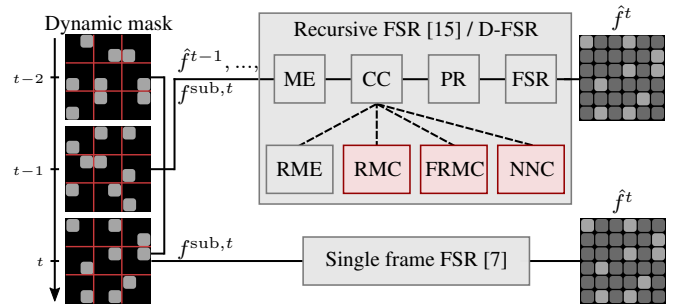


Fig. 1: Flow diagram of quarter sampling for video data using a dynamic mask. Our novel contributions to the consistency checks of recursive FSR are highlighted in red. Abbreviations: ME: Motion estimation, CC: Consistency check, PR: Projection, RME: Reverse motion estimation, RMC: Reverse motion check, FRMC: Fast reverse motion check, NNC: Nearest neighbor check.

tion has been investigated for fixed quarter sampling masks [14, 15] as well as for dynamic quarter sampling masks [16]. For the latter, the sampling mask changes from frame to frame and a sophisticated read-out strategy is applied such that each pixel in a 2×2 block is read exactly once within four frames. Every fourth frame, the mask repeats. Compared to a purely spatial or purely temporal sub-sampling, a more uniform placement of the pixels in time and space is achieved and a higher reconstruction quality is found [16]. In this paper, we consider both fixed and dynamic masks.

Among those works, causal reconstruction algorithms such as the one in [15] are of special interest since they only use past measurements for the reconstruction of the current frame. Such causal scenario is of special importance since future measurements are not available in real-time applications at the time of the reconstruction. To processing chain of the measurement an reconstruction is illustrated in Figure 1 for a current frame at time t and two preceding frames.

In this paper, we focus on such causal reconstruction scenarios as it is done in [15]. Our novel contributions to these scenarios are twofold: As first contribution, we propose a novel combination of consistency checks that finds outliers among the motion vectors much faster and more reliable than in [15]. This is marked with red color in Figure 1. As second contribution, we propose the so called D-FSR being a new implementation of recursive FSR that handles the projected pixel differently than in [15] and can be used with dynamic sampling masks. It is different to [15], where only fixed masks are considered and it is different from [16], where information from future frames is used.

Our analysis is performed on a variety of test sequences to show the wide applicability of the modifications. Besides analysis of the

reconstruction quality of the proposed modifications, visual comparisons are provided, and the computation times are compared. This paper is organized as follows: In Section 2, we present the state of the art. In Section 3, we describe our novel contributions. In Section 4, the simulation results are presented and discussed. Section 5 summarizes the paper.

2. STATE OF THE ART

2.1. Single Frame Reconstruction

In order to reconstruct the missing pixels from the sampled image data, frequency selective reconstruction (FSR) has shown to provide high reconstruction quality outperforming other reconstruction techniques [7]. The sub-sampled image can be understood as $f_{mn}^{\text{sub}} = f_{mn} \cdot b_{mn}$, where f and b are the reference high resolution image and the binary mask. From the sub-sampled image and the mask, FSR reconstructs an image \hat{f}_{mn} . It therefore subdivides the image into neighboring blocks that are reconstructed using the measurements from their neighboring blocks, too. The model of each block is build in the Fourier domain where the image is assumed to be approximately sparse [17, 18].

2.2. Recursive FSR

For video data, it was proposed to additionally use information from previous frames [15]. For any missing pixel in the current frame, a motion vector pointing to a measured pixel in one of the preceding frames could provide useful information. In [15], Jonscher et al. propose such an approach called recursive FSR (R-FSR). In R-FSR, the motion estimation is performed by a pixel-wise template matching using the already reconstructed past frames and the measured data from the current frame. Such motion vector field is illustrated in Figure 2(a). During the template matching [19], some motion vectors may be untrustworthy. This can result from cases where the motion is larger than the search range, from occlusions or local optima. Since non-regularly sampled data is used, these issues are increased further as fewer information is available.

In order to sort out unfavorable motion vectors, Jonscher et al. propose a consistency check for which the motion vectors in the reverse direction are calculated using an additional reverse motion estimation (RME). Only when both motion vectors coincide, the motion vector is accepted. While this strategy is reasonable and seems successful, it is also computationally demanding since the number of cost functions that needs to be evaluated is doubled.

With the accepted motion vectors at hand, values for some of the missing pixels the current frame can be found by following their motion vector into the past. If a measurement is available at the corresponding position in the past frame, it is projected to the current frame and it is used as an additional measurement during the reconstruction. In case projections from more than one past frame are available, these are averaged.

3. NOVEL CONTRIBUTIONS

Our novel contributions to the recursive reconstruction of non-regularly sampled video data are twofold and described in the two following sub-sections.

3.1. Proposed Consistency Checks

As first contribution, we propose two novel consistency checks. Their aim is to achieve a reduced computational complexity and to increase the reconstruction quality.

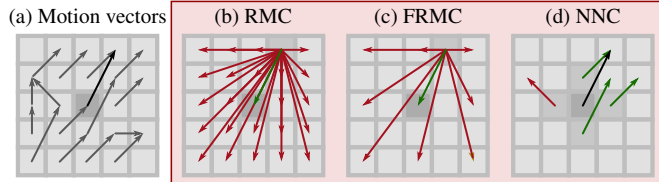


Fig. 2: Illustration of (a) the motion vector field from frame $f^{(t)}$ to frame $f^{(t-1)}$ and (b-d) the used consistency checks. In contrast to the values used in the text, RMC is shown for a search range of $\{-2, -1, 0, -1, 2\}$ and FRMC is shown for a partial search range being $\{-2, 0, 2\}$.

3.1.1. Fast Reverse Motion Check (FRMC)

The first proposed consistency check is related to RME. Instead of calculating the reverse motion vector field, we test the more relevant motion vectors around the already found motion vector. In a first step, we therefore propose testing the same number of motions vectors as in RME but placing them symmetrically around the motion vector pointing back to the original pixel. This is illustrated in Figure 2(b) and is further denoted as reverse motion check (RMC). This algorithm can be assumed to be roughly as fast as RME since the same number cost functions needs to be calculated.

In a second step, we propose testing only a tiny subset of these motion vectors leading to fast RMC (FRMC). In case of an untrustworthy motion vector, the probability is high that many of the motion vectors in the reverse direction have a smaller cost than the currently chosen motion vector. In our setup, we test only motions in the set $\{-7, -3, -1, 0, 1, 3, 7\}$ for both spatial dimensions instead of the testing all motion vectors $\{-9, -8, \dots, 9\}$ as in RMC and RME. The number of motions to be tested is significantly reduced from 361 to 49. An example is illustrated in Figure 2(c). If the green arrow has the lowest cost, the motion is accepted. If any of the red arrows has the lowest cost, the motion is rejected.

3.1.2. Nearest Neighbor Check (NNC)

The second proposed consistency check does not require any additional template-matching at all and is therefore potentially faster. It is supposed to be used in combination with FRMC in order to speed up the calculations. This can be achieved since many motion vectors may already be sorted out with this simpler consistency check. It relies on testing the consistency of the determined vector field in a local neighborhood. Denoting the found motion vector field as $(\alpha_{mn}, \beta_{mn})$, we perform a 3×3 median filtering for the two individual components resulting in the filtered motion vector field

$$(\tilde{\alpha}_{mn}, \tilde{\beta}_{mn}) = (\text{median}_{3 \times 3}(\alpha_{mn}), \text{median}_{3 \times 3}(\beta_{mn})). \quad (1)$$

Next, for each position (m, n) , the filtered motion vectors at the four nearest neighboring positions $(m-1, n)$, $(m+1, n)$, $(m, n-1)$, and $(m, n+1)$ are compared. Only if the sum of the absolute differences of the motion vectors is at most one for each neighboring pair, the motion is accepted. If not, the motion is rejected because it is considered to be untrustworthy. Such accepted/rejected motions are highlighted with green/red color in Figure 2(d). This modification of the consistency check is abbreviated as nearest neighbor-check (NNC) later on.

3.2. Proposed Recursive FSR for Dynamic Masks (D-FSR)

As second contribution to this paper, we propose a new implementation of a recursive FSR build upon the work from [15]. Other than R-FSR from [15], our implementation handles the projected



Fig. 3: Frame 20 of each video sequence used for the simulations.

pixels differently and is capable of additionally handling dynamic masks. The novel algorithm is abbreviated as D-FSR. During the model generation, we use the projected pixels in the same manner as R-FSR. As a last step, however, the model found during the reconstruction is to be overwritten with the available measurements as commonly done in FSR [7]. In this step, R-FSR makes no difference between measured and projected pixels, whereas D-FSR considers the projected pixels to be less reliable and therefore does not use them to overwrite the model.

4. SIMULATIONS AND RESULTS

In this section, we evaluate the performance of the proposed consistency checks and D-FSR. We compare them to R-FSR + RME from [15], investigate the impact of using a dynamic mask instead of a fixed mask, and show the runtimes. For any reconstructions with FSR, we chose the same parameters as in [15] except for the concealed weighting of the FSR being set to zero allowing us to perform a fully parallel processing of all blocks during the reconstruction. For all recursive reconstructions, we use three previous frames for the motion estimation and projection. For R-FSR + RME from [15] we use raw simulation data kindly provided by the authors. This data is available for the fixed mask and one of the test sequence. For all other cases we use our own implementations as described in Section 3.

For the test sets, we use several monochrome video sequences: The first 100 frames of the *Spincalendar* sequence having a resolution of 1280×720 pixels are used since these were also used in [15]. Further video data is taken from the *JVET* test sequences [20]. For the *JVET - ClassC* sequences, the resolution is 832×480 pixels and we use the first 50 frames. Moreover, we chose three sequences from *JVET - A*. For those, we spatially down-scaled the frames by a factor of three resulting in 1280×720 pixels to achieve a similar resolution as for the other sequences. Once more, we use the first 100 frames. Figure 3 depicts a single frame of each used sequence.

To evaluate the quality of the reconstructed videos, we calculate the frame-wise PSNR and average it for all frames of the respective video. For the PSNR calculation, a border of 40 pixels is omitted since boundary effects are not considered to be of interest in our evaluation. The PSNR values are then further averaged across the video sequences to achieve a meaningful average value. The same evaluations were done for the mean structural similarity (SSIM) [21].

Tables 1 and 2 show the results of the reconstruction quality in terms of PSNR using a fixed and a dynamic mask, respectively. Besides the results using the single frame FSR [7], the various consistency checks are shown in combination with D-FSR. Additionally, the SSIM was evaluated in the same manner. Its results are in accordance with the PSNR values and the averages are provided in the last row of Tables 1 and 2 for completeness. Comparing the average results from both tables, we find that using a dynamic mask outperforms using a fixed mask by roughly +1 dB which is consistent with the findings in [16].

Table 1: Results for the fixed mask. The average reconstruction quality in terms of PSNR in dB is provided using different test sets. For the averages, SSIM is provided, too.

(fixed mask)		FSR [7]	R-FSR + RME [15]	D-FSR + RME	D-FSR + RMC	D-FSR + FRMC	D-FSR + FRMC + NNC
	Spincalendar	30.38	31.66	32.67	32.72	33.00	32.68
Class C	BasketballDrill	31.27	-	31.10	31.44	31.38	31.44
	BQMall	27.49	-	27.73	27.81	27.82	27.81
	PartyScene	23.22	-	23.35	23.37	23.37	23.39
	RaceHorses	28.69	-	28.32	28.96	28.85	29.15
A	Tango2	39.80	-	37.78	40.58	40.40	40.62
	ParkRunning3	30.16	-	31.21	31.27	31.19	31.43
	FoodMarket4	47.23	-	41.83	46.53	45.72	46.35
Average (PSNR)		32.28	-	31.75	32.83	32.72	32.86
Average (SSIM)		0.9334	-	0.9368	0.9399	0.9394	0.9406

Table 2: Results for the dynamic mask. The average reconstruction quality in terms of PSNR in dB is provided using different test sets. For the averages, SSIM is provided, too.

(dynamic mask)		FSR [7]	D-FSR + RME	D-FSR + RMC	D-FSR + FRMC	D-FSR + FRMC + NNC
	Spincalendar	30.43	33.20	33.26	33.56	33.21
Class C	BasketballDrill	31.30	33.62	34.28	34.37	34.31
	BQMall	27.53	30.01	30.14	30.39	30.27
	PartyScene	23.23	24.64	24.70	25.05	24.92
	RaceHorses	28.71	28.34	29.02	28.92	29.22
A	Tango2	39.84	37.59	40.69	40.51	40.73
	ParkRunning3	30.19	31.36	31.42	31.34	31.58
	FoodMarket4	47.28	41.56	46.58	45.78	46.38
Average (PSNR)		32.31	32.54	33.76	33.74	33.83
Average (SSIM)		0.9338	0.9477	0.9510	0.9520	0.9524

In Table 1, we can observe that D-FSR + RME, outperforms the original version from [15] by +1.01 dB for the *Spincalendar* sequence. Beyond this, we investigated the influence of the proposed consistency checks on the reconstruction quality in terms of PSNR. Using RMC, the reconstruction quality averaged over all used sequences is increased by +1.08 dB for the fixed mask and +1.22 dB for the dynamic mask. Using the fast variant of RMC, namely FRMC, results in a slight decrease of the average PSNR. Interestingly, this trend is not uniform across the different sequences. For example, the *FoodMarket4* scene shows a relevant loss whereas the reconstruction for other sequences improves. The average loss is reasonable, as not all motion vector are tested in the opposite direction. Lastly, the NNC is added to the FRMC. This combination shows the highest average reconstruction quality in both Tables 1 and 2. For the dynamic mask, a gain of +1.52 dB is observed compared to the single frame FSR [7] and a gain of +1.29 dB is observed compared to D-FSR + RME. This means, that FRMC + NNC overcomes the loss arising from switching to FRMC and even improves the quality in average.

For a more in-depth view of the simulated data, Figure 5 shows the frame-wise PSNR gain relative to the single frame FSR. The *Spincalendar* sequence is used. It can be seen that roughly 10 frames are needed for the recursive algorithm to converge to a good quality and that the gain is then mostly constant for all the remaining frames.

In order to be able to judge the visual quality, Figure 4 shows two sections of the reconstructed frames using the dynamic mask. For the example from the *Tango2* sequence, it can clearly be seen that the rather low average PSNR of D-FSR + RME arises from strong artifacts indicated by the red arrow. These arise from faulty motion vectors that can occur in nearly constant regions in combination with

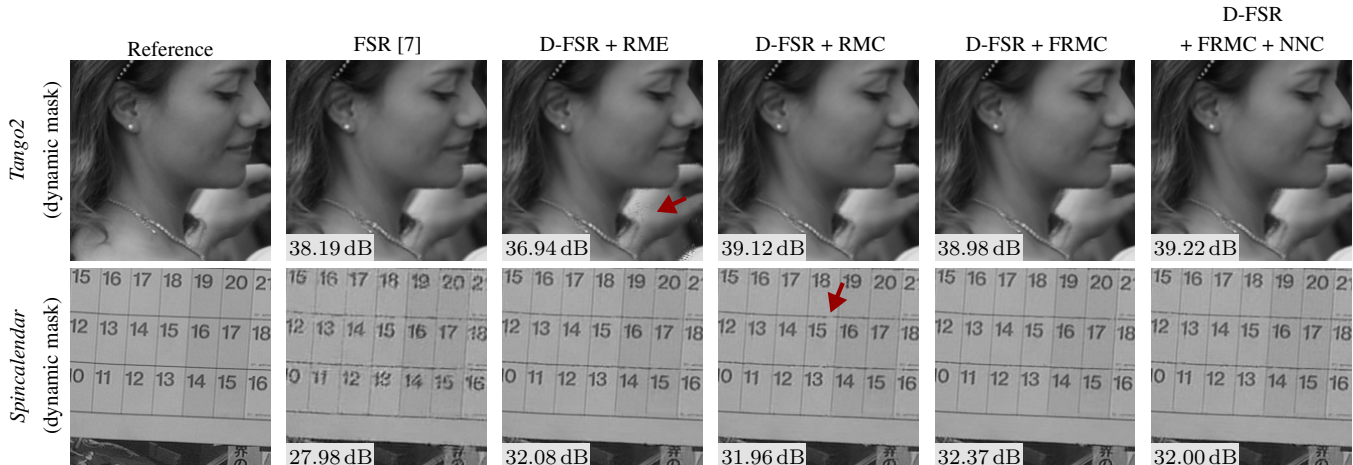


Fig. 4: Visual comparison of the different reconstruction methods for sections of frame 20 from the *Tango2* sequence and frame 30 from the *Spincalendar* sequence. The PSNR values given as insets are calculated for the visible sections. Since only dynamic masks are used, data for R-FSR+RME [15] is not available. (Best to be viewed enlarged on a monitor.)

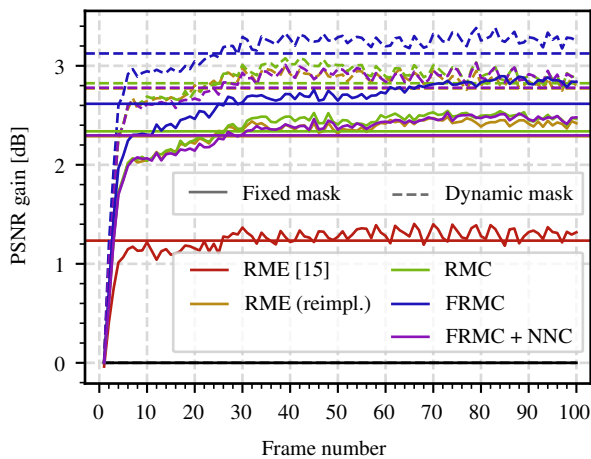


Fig. 5: Frame-wise gain of the reconstruction quality in terms of PSNR relative to the single frame FSR [7] using the *Spincalendar* sequence.

large motion vectors and should be sorted out. For the other consistency checks, these motion vectors are sorted out as desired. For the *Spincalendar* sequence, the differences among the proposed algorithms are more subtle. The cases where RMC performs slightly worse than FRMC + NNC are highlighted with red arrows.

In addition to the reconstruction quality, we evaluate the computation times for the different algorithms in case of the dynamic masks. We provide the runtimes for the motion estimation, the consistency checks between the current frame and its last three frames, and the reconstruction. For the motion estimation a fast variant using the GPU was developed, too. For the motion estimation and consistency checks, we restrict the executions to a single core on an Intel i9-10980XE CPU with 3.00GHz. Table 3 summarizes the results. Timings for R-FSR + RME from [15] are not available but its algorithmic complexity is identical to that of D-FSR + RME.

The code for the pixel-wise motion estimation is identical for all three cases and therefore the results are all close. The same is true for the FSR. The slight differences can be used as an estimate of the accuracy of the measurements and are considered to be acceptable. Taking a look at the runtimes of the consistency checks, we can see

Table 3: Runtimes of the different steps in seconds. The algorithmic complexity of R-FSR + RME from [15] is identical to that of D-FSR + RME. ME: Motion estimation, CC: consistency check.

	ME	CC	FSR	Total
D-FSR + RME	21.56	33.80	6.02	61.37
D-FSR + RMC	23.11	40.19	6.11	69.41
D-FSR + FRMC	21.49	21.02	6.05	48.56
D-FSR + NNC + FRMC	23.14	2.56	6.07	31.77

that NNC + FRMC is more than 13-fold faster than the RME and RMC. Remarkably, combining FRMC and NNC, is more than 8-fold faster than using solely the very fast NNC. In such cases, the slower FRMC is skipped. It is worth taking these times into relation with the total runtimes of the reconstruction, where an overall reduction of -48% is achieved.

5. CONCLUSION

Using recursive reconstruction algorithms, a pixel-wise motion estimation and projection between the current frame and its preceding frames is performed to enhance the reconstruction quality of the current frame. Since some motion vectors may be untrustworthy, it is required to perform a consistency check which sorts out such motion vectors. For this task, R-FSR from [15] relies on a computationally expensive reverse motion estimation (RME). In order to reduce the cost, we propose a new consistency check which is a combination of FRMC and NNC. Altogether, more relevant reverse motion vectors are tested in FRMC and most evaluations are skipped by comparing the locally neighboring motion vectors using NNC. The proposed D-FSR uses the projected pixels differently and can handle dynamic masks as well.

With our proposed recursive reconstruction method and consistency checks, D-FSR + FRMC + NNC, we achieve a +1.01 dB higher reconstruction quality in terms of PSNR compared to R-FSR + RME from [15] in case of the fixed mask and the *Spincalendar* sequence. Testing a larger dataset of different video sequences, we find that the D-FSR + FRMC + NNC performs better than D-FSR + RME by 1.29 dB in average for the dynamic mask. The average PSNR gain with respect to the single frame FSR [7] is +1.52 dB. At the same time, the proposed consistency check, is 13-fold faster than RME which reduces the total runtime by -48% .

6. REFERENCES

- [1] Michael Schöberl, Jürgen Seiler, Siegfried Foessel, and André Kaup, “Increasing imaging resolution by covering your sensor,” in *Proc. 18th IEEE International Conference on Image Processing*, Brussels, Sept. 2011, pp. 1897–1900.
- [2] Mark A. Z. Dippé and Erling Henry Wold, “Antialiasing through stochastic sampling,” in *Proc. 12th Annual Conference on Computer Graphics and Interactive Techniques*, New York, July 1985, pp. 69–78.
- [3] Gilles Hennenfent and Felix J. Herrmann, “Irregular sampling: from aliasing to noise,” in *Proc. 69th EAGE Conference and Exhibition*, London, June 2007, pp. cp–27–00063.
- [4] Yui Maeda and Junichi Akita, “A CMOS image sensor with pseudorandom pixel placement for clear imaging,” in *Proc. International Symposium on Intelligent Signal Processing and Communication Systems*, Kanazawa, Dec. 2009, pp. 367–370.
- [5] Joaquin Lopez Herraiz, Samuel Espana, Esther Vicente, Elena Herranz, Manuel Desco, Juan Jose Vaquero, and Jose Udias, “Frequency selective signal extrapolation for compensation of missing data in sinograms,” in *Proc. IEEE Nuclear Science Symposium Conference Record*, Dresden, Oct. 2008, pp. 4299–4302.
- [6] Thomas Stehle, “Removal of specular reflections in endoscopic images,” *Acta Polytechnica*, vol. 46, no. 4, pp. 32, 2006.
- [7] Jürgen Seiler, Markus Jonscher, Michael Schöberl, and André Kaup, “Resampling images to a regular grid from a non-regular subset of pixel positions using frequency selective reconstruction,” *IEEE Transactions on Image Processing*, vol. 24, no. 11, pp. 4540–4555, Nov. 2015.
- [8] Simon Grosche, Jürgen Seiler, and André Kaup, “Iterative optimization of quarter sampling masks for non-regular sampling sensors,” in *Proc. International Conference on Image Processing 2018*, Athens, Oct. 2018, pp. 26–30.
- [9] Emmanuel Candes, Justin Romberg, and Terence Tao, “Robust uncertainty principles: exact signal reconstruction from highly incomplete frequency information,” *IEEE Transactions on Information Theory*, vol. 52, no. 2, pp. 489–509, Feb. 2006.
- [10] David L. Donoho, “Compressed sensing,” *IEEE Transactions on Information Theory*, vol. 52, no. 4, pp. 1289–1306, Apr. 2006.
- [11] Simon Grosche, Andy Regensky, Jürgen Seiler, and André Kaup, “Boosting compressed sensing using local measurements and sliding window reconstruction,” *IEEE Transactions on Image Processing*, vol. 29, pp. 7931–7944, 2020.
- [12] Stéphane Mallat and Zhifeng Zhang, “Matching pursuits with time-frequency dictionaries,” *IEEE Transactions on Signal Processing*, vol. 41, no. 12, pp. 3397–3415, 1993.
- [13] Joel A. Tropp and Anna C. Gilbert, “Signal recovery from random measurements via orthogonal matching pursuit,” *IEEE Transactions on Information Theory*, vol. 53, no. 12, pp. 4655–4666, Dec. 2007.
- [14] Markus Jonscher, Jürgen Seiler, Michel Bätz, Thomas Richter, Wolfgang Schnurrer, and André Kaup, “Reconstruction of Videos Taken by a Non-Regular Sampling Sensor,” in *Proc. International Conference on Visual Communications and Image Processing*, Singapore, Dec. 2015, pp. 1–4.
- [15] Markus Jonscher, Karina Jaskolka, Jürgen Seiler, and André Kaup, “Recursive Frequency Selective Reconstruction of Non-Regularly Sampled Video Data,” in *Proc. Picture Coding Symposium*, Nuremberg, Germany, Dec. 2016, pp. 1–5.
- [16] Markus Jonscher, Jürgen Seiler, Daniela Lanz, Michael Schöberl, Michel Batz, and André Kaup, “Dynamic non-regular sampling sensor using frequency selective reconstruction,” *IEEE Transactions on Circuits and Systems for Video Technology*, pp. 1–1, 2018.
- [17] Edmund Y. Lam and Joseph W. Goodman, “A mathematical analysis of the DCT coefficient distributions for images,” *IEEE Transactions on Image Processing*, vol. 9, no. 10, pp. 1661–1666, Oct. 2000.
- [18] Michael Elad, Mário A. T. Figueiredo, and Yi Ma, “On the role of sparse and redundant representations in image processing,” *Proceedings of the IEEE*, vol. 98, no. 6, pp. 972–982, June 2010.
- [19] Roberto Brunelli, *Template matching techniques in computer vision: theory and practice*, John Wiley & Sons, 2009.
- [20] Frank Bossen, Jill Boyce, Karsten Suehring, Xiang Li, and Vadim Seregin, “JVET common test conditions and software reference configurations for SDR video,” document, JVET-N1010-v1, Joint Video Exploration Team (JVET), Mar. 2019.
- [21] Zhou Wang, Alan Conrad Bovik, Hamid Rahim Sheikh, and Eero P. Simoncelli, “Image quality assessment: From error visibility to structural similarity,” *IEEE Transactions on Image Processing*, vol. 13, no. 4, pp. 600–612, Apr. 2004.